17th AIAA/CEAS Aeroacoustics Conference (32nd AIAA Aeroacoustics Conference)
05 - 08 June 2011, Portland, Oregon

AIAA 2011-2830

Experimental Investigations of Coherence Based Noise Source Identification Techniques for Turbomachinery Applications - Classic and Novel Techniques

Ian Davis* Gareth J. Bennett†

Trinity College Dublin, Ireland.

Coherence based noise source identification techniques utilise the ordinary linear coherence function between two signals to identify the contribution of one or more sources to the noise measured at a location of interest. Such techniques can assess the relative contributions of broadband noise sources, which are the dominant noise sources in turboshaft engines, to the sound radiated at a far-field location. All such techniques require the placement of dynamic pressure sensors close to these sources. Experimental studies undertaken at the Engine Acoustics Branch of the German Aerospace Agency, DLR, as part of an EU FP7 project, TEENI, have provided data for a range of test scenarios. The test rig has been designed to represent the key acoustic elements of a real turboshaft engine. Each noise source identification technique were applied in a two noise source region scenario. The aim of these techniques was to identify the contribution of one or both of these noise sources to the noise measured at a sensor of interest. Test set-ups where each source is present in isolation were also investigated to provide benchmark auto-spectra. These benchmarks are compared to the resulting spectra from several coherence based techniques in order to assess each technique's efficacy in identifying the relative contribution of one or both source region(s) to the noise measured by a receiver of interest. A modal CSA technique is also proposed and tested, based on the five-microphone conditional spectral analysis technique, which uses decomposed acoustic modes at the duct inlet to identify the contribution of both of the source region(s) to the amplitudes of the modes propagating at the inlet end of the duct. The novel technique was tested for broadband noise source identification, by investigating how accurately it could identify the contributions of two broadband noise source regions to the modal content at the duct inlet.

I. Introduction

Broadband noise generation has become a subject of significant interest in the design of turbomachinery in recent years. For aeroengines and turboshaft engines, exhaust broadband noise is produced at the many rotor-stator stages of the turbines and by the combustor stage in direct and indirect (also called entropy noise) form. This noise is usually a significant contributor to the overall sound level during aircraft landing. Coherence based noise-source identification techniques can be used to identify the contribution of core noise to near and far field acoustic measurements in turbomachinery. The coherent output power technique, reported initially by Halvorsen and Bendat,[1] has been reported extensively in aeroacoustics literature utilising the ordinary coherence function between internal measurements at a source and far-field measurements. Chung's[2] flow noise rejection technique (signal enhancement), using three microphones to remove extraneous noise from a far-field measurement of a single noise source, was used by Shivashankara[3] to identify the internal core noise contribution to far-field measurements. A partial coherence technique was developed by Hsu and Ahuja[4] using five microphones which can separate out the contributions of two sources in the presence of extraneous noise. Previously published work in this area from the 1970's and 1980's has been revisited in more recent years by Minami and Ahuja[5] and Nance.[6] In Bennett and Fitzpatrick[7] techniques which can be used to identify the contribution of combustion noise to near and far-field acoustic measurements of aero-engines

*Ph.D. Student, Dept. of Mechanical and Manufacturing Engineering, Trinity College, Dublin 2, Ireland.
†Lecturer, Dept. of Mechanical and Manufacturing Engineering, Trinity College, Dublin 2, Ireland.

were evaluated. In the papers by Bennett and Fitzpatrick[8] and by Bennett et al[9,10] analysis techniques which allow the contribution of linear and non-linear mechanisms to the propagated sound to be identified was reported for tonal and narrow band noise respectively.

II. Classic Coherence Based Noise Source Identification Techniques

Consider the scenario depicted in Fig. 1, which is a simplified model of two source regions in a duct, S_1 and S_2. S_1 is a turbine and S_2 is a combustor. Acoustic pressure sensors are located close to both source regions. This scenario represents the simplified acoustics of a turboshaft engine. Many so called "classic" techniques of noise source identification exist in the literature. These techniques can be used to identify the contribution of the noise generated by these noise sources to the sound radiated to a far-field location of interest. Several such techniques have been investigated as part of this study. The magnitude squared or ordinary coherence function is the principal tool used in all these techniques. The coherence function of two time-domain signals $x(t)$ and $y(t)$ can be found by first transforming blocks of the signals into the Fourier domain, giving $X(f)$ and $Y(f)$. The power spectral densities ($G_{xx}(f)$ and $G_{yy}(f)$) and cross-spectral density ($G_{xy}(f)$) of these Fourier domain blocks can then be formed. The dependence on frequency will be dropped from this point on for succinctness. By averaging these auto and cross-spectra over many signal blocks, the coherence function between $x(t)$ and $y(t)$ can be found by:

$$\gamma_{xy}^2 = \frac{|G_{xy}|^2}{G_{xx}G_{yy}} \leq 1 \tag{1}$$

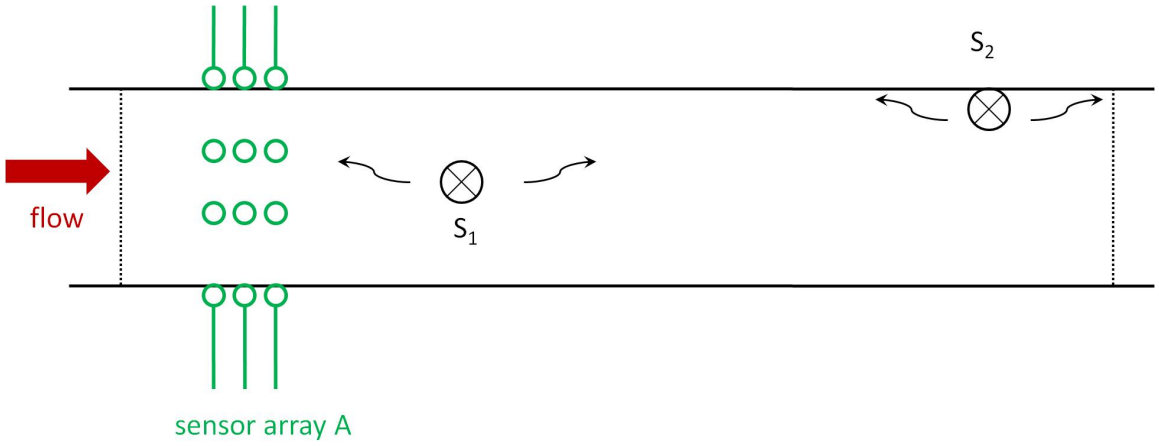

Figure 1: Simplified representation of acoustics inside a turbomachinery duct. Sound waves are emitted by S_1 and S_2, which represent a turbine and combustor stage respectively, and propagate in the duct. When the turbine is rotating, a flow is induced in the duct.

If the coherence function is greater than zero but less than unity, one of three possible physical situations exist:

1. Extraneous noise is present in the measurements.
2. The system relating $x(t)$ and $y(t)$ is not linear.
3. $y(t)$ is an output due to input $x(t)$ as well as other inputs.

A. Coherent Output Power (COP)

In the case where a pure source time-domain measurement $x(t)$ is available (pure meaning that no extraneous noise, such as additional noise sources, is measured by this sensor), and an output measurement $y(t)$ is available which measures this source as well as extraneous noise (which could include other sources), the contribution of the source measured by $x(t)$ to the noise measured by $y(t)$ is given by:

$$G_{vv} = G_{yy}\gamma^2_{xy} \tag{2}$$

where $v(t)$ is the contribution of the source measured by $x(t)$ to $y(t)$. This result is known as the coherent output spectrum. With reference to the scenario shown in Figure 1, and given that a pure source measurement is available at S_2, the coherent output power technique model would be represented as shown in Figure 2. $y(t)$ could be a measurement in the duct, or a far-field measurement outside of the turboshaft engine.

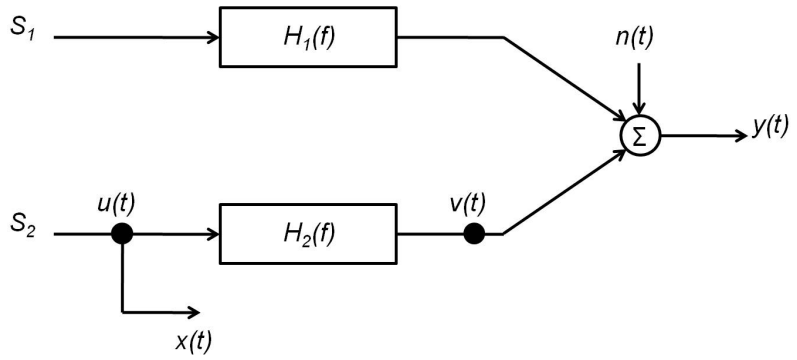

Figure 2: Coherent output power model for scenario shown in Fig. 1 with a pure source measurement of S_2.

If extraneous noise is present in the source measurement $x(t)$, which will be denoted by $m(t)$, the coherent output spectrum is affected as follows:

$$G_{v'v'} = G_{yy}\gamma^2_{x'y} = G_{vv}\frac{G_{xx}}{G_{xx}+G_{mm}} \leq G_{vv} \tag{3}$$

i.e. the technique will underestimate $v(t)$. In the scenario shown in Figure 1, and given that $x(t)$ is a measurement at the source S_1, the COP model will be as shown in Figure 3. As the rotor induces a flow in the duct, the source measurement $x(t)$ in this case will measure both S_1 and extraneous noise $m(t)$. For the scenario shown in Figure 1, this induced flow will generate flow noise. This flow noise is caused by noise sources distributed in the turbulent fluid, and also the hydrodynamic interaction between the fluid flow and the pressure sensor. This flow noise will contribute to this extraneous noise, and assuming that no other noise sources are present in the test duct, could be the main contributor of extraneous noise not correlated between the sensors.

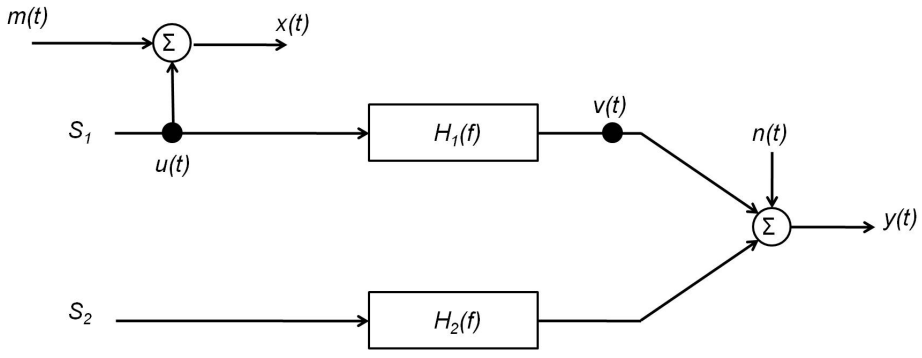

Figure 3: COP model for scenario shown in Fig. 1 with source measurement at S_1. The presence of extraneous flow noise at the inlet measurement will diminish the efficacy of the technique, as shown in Eq. 3

B. Signal Enhancement (SE)

Unlike the COP, which requires a pure measurement of the source of interest without extraneous noise, Chung[2] developed a technique for extraneous noise rejection at the input using a minimum of three measurements. This technique can therefore be applied when a pure measurement at the source is not possible, provided this extraneous noise is uncorrelated between each measurement. Such extraneous noise could be flow noise for example. The desired spectra can then be found using these equations (shown for one sensor only as an example):

$$G_{v_1 v_1} = G_{y_1 y_1} \frac{|\gamma_{y_1 y_2}||\gamma_{y_1 y_3}|}{|\gamma_{y_2 y_3}|} = \frac{|G_{y_1 y_2}||G_{y_1 y_3}|}{|G_{y_2 y_3}|} \tag{4}$$

$$G_{n_1 n_1} = G_{y_1 y_1} - G_{v_1 v_1} \tag{5}$$

With reference to Figure 1, and given that three sensors ($y_1(t)$, $y_2(t)$ and $y_3(t)$) measure source S_1 plus uncorrelated extraneous noise, the SE model may be be as shown in Figure 4. The presence of S_2 in the extraneous noise $l_k(t)$ terms is shown, as the sensors located at S_1 will also measure S_2's contribution to the noise at these locations. If this is the case, the measurement of the contribution of S_2 must be uncorrelated between each sensor, in which case S_2 will be measured as uncorrelated noise and will not contaminate the results.

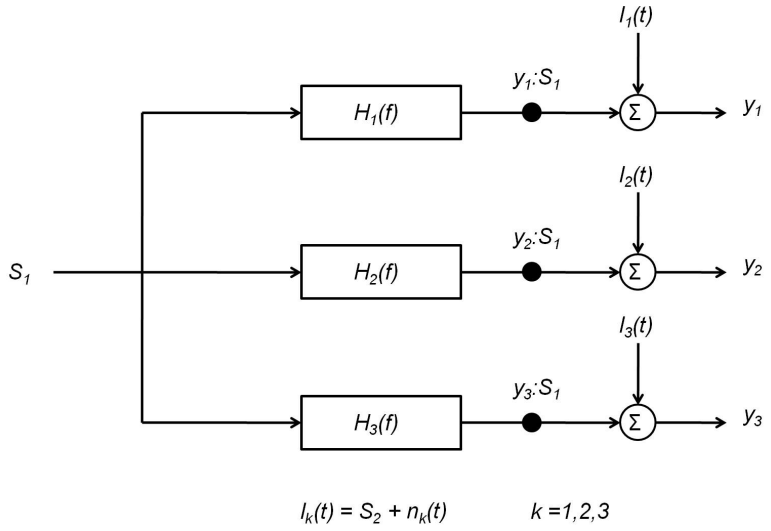

Figure 4: Signal enhancement model for scenario shown in Fig. 1 with three measurements of S_1 with additional uncorrelated extraneous noise.

C. Conditional Spectral Analysis (CSA)

One of the limitations of the SE technique is that for measurement locations within the same pressure field, the technique may only be applied when there is a single correlated source between the records. Minami and Ahuja[5] discuss the errors resulting from using the signal enhancement technique when two sources, as opposed to only one source, are measured with extraneous noise. For the situation where there are only two correlated sources, and a pure measure of one of them is attainable, the COP and the SE techniques may be used in conjunction with each other with conditional spectral analysis to successfully identify both sources and the extraneous noise. This approach is presented by Hsu and Ahuja.[4] This problem case is shown in Figure 5(a) for the scenario shown in Figure 1. In this scenario, a pure source measurement is available at S_2, but not at S_1. The first stage consists of separating out the part correlated with the measurable source (S_2), using the COP technique, and thus identifying its contribution. The second stage uses a partial coherence formulation of the SE technique on the residual to remove the extraneous noise, as demonstrated in Figure 5(b). Assuming a pure measurement of source S_2 is available, only four microphones are required,

with this source measurement used as an input. The other three microphones measure a combination of contributions from both source S_1 and S_2. In the case that a pure measurement of S_2 is not available, two sensor measurements can be used at S_2 instead of a single measurement. It is required that these microphone measurements measure S_2 and extraneous noise only, and that this extraneous noise is uncorrelated between all sensor measurements. This is the five-microphone CSA technique.

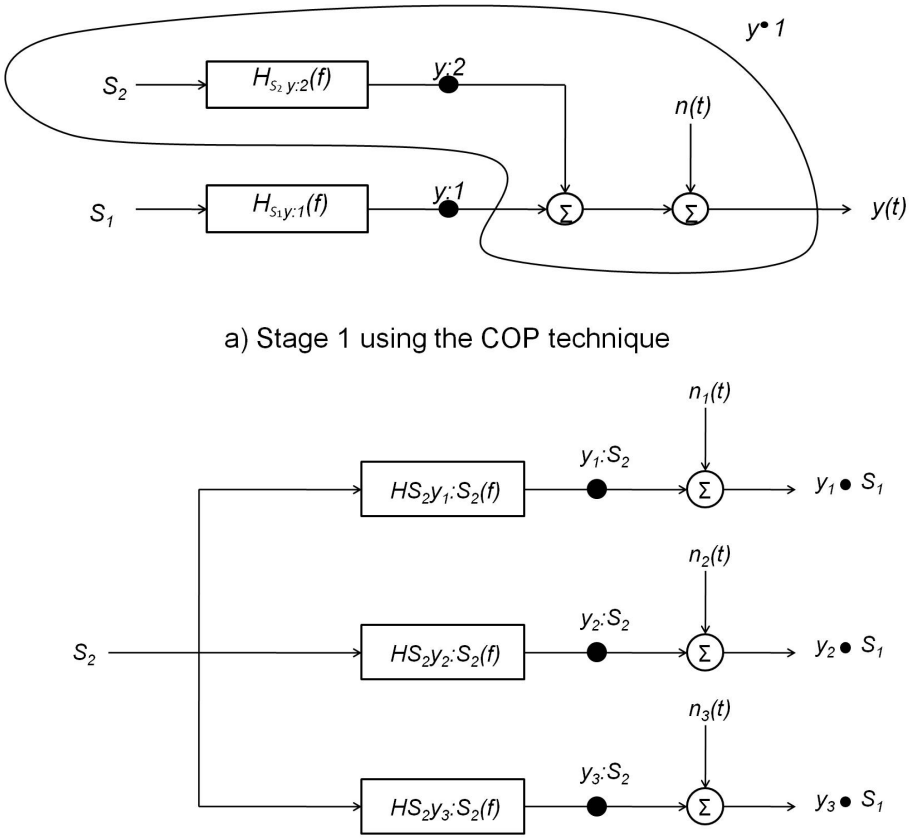

Figure 5: Conditional Spectral Analysis Model for scenario shown in Fig. 1.

Figure 6 shows the five-microphone CSA model for the test scenario described in Figure 1. It should be noted that microphone measurements $y_4(t)$ and $y_5(t)$ are such that they measure the single source S_2 and uncorrelated noise only. The other three output sensors can be located anywhere, provided their measurements of S_1 and S_2 are correlated with one another. The source spectra G_k and G_v can be found using the following equations (for $y_1(t)$ only with dependence on frequency not shown for brevity):

$$G_{k_1k_1} = \frac{|G_{y_1y_2} - \frac{G_{y_1y_4}G_{y_5y_2}}{G_{y_5y_4}}||G_{y_1y_3} - \frac{G_{y_1y_4}G_{y_5y_3}}{G_{y_5y_4}}|}{|G_{y_2y_3} - \frac{G_{y_2y_4}G_{y_5y_3}}{G_{y_5y_4}}|} \tag{6}$$

$$G_{v_1v_1} = \frac{G_{y_1y_4}G_{y_1y_5}}{G_{y_4y_5}} \tag{7}$$

III. The CSA Modal Technique

A new modal based technique is proposed and investigated in this study. This technique identifies the contribution of two noise sources to the modal content at a location of interest. The technique proposed is an enhancement of the five-microphone conditional spectral analysis technique discussed in section II. The

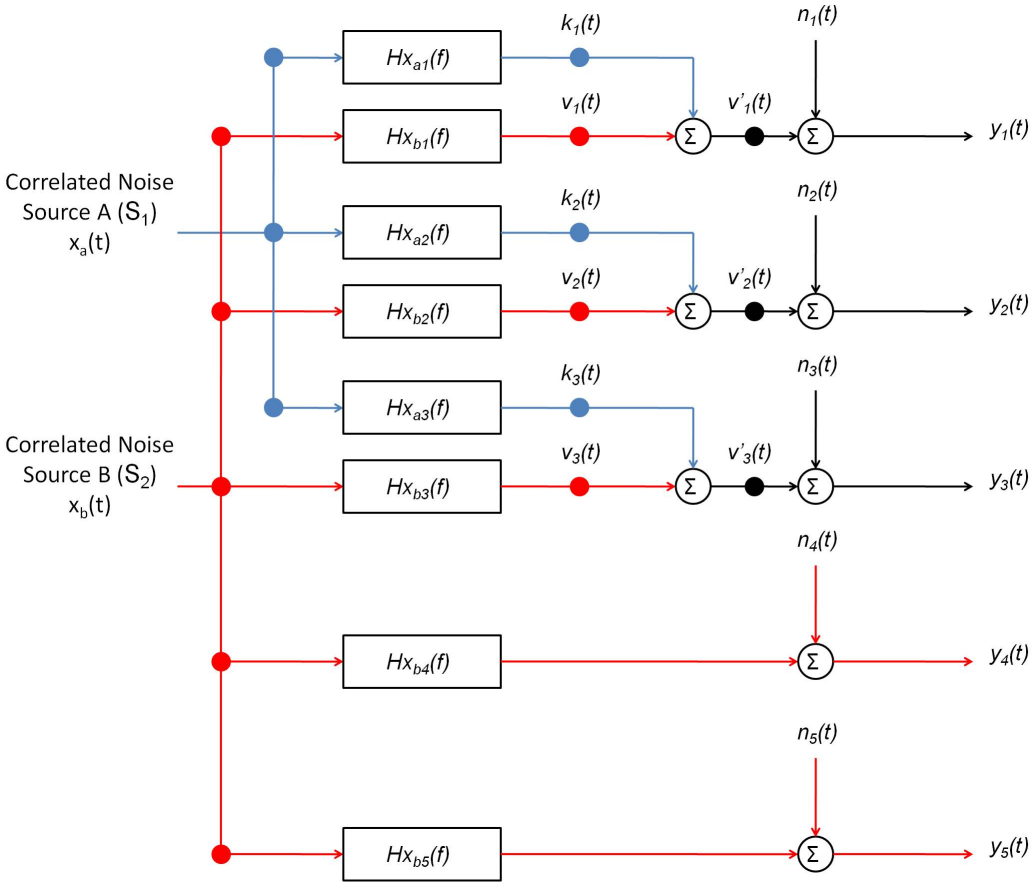

Figure 6: Five-Microphone CSA Technique Model for scenario shown in Fig. 1.

hypothesis is that the auto and cross-spectra used to formulate the k and v spectra in the five microphone technique can be calculated using the complex Fourier domain signals of the original time-domain signals $x_1(t)$-$x_5(t)$. Given that $x_1(t)$-$x_5(t)$ are microphone measurements of the acoustic pressure with time, the Fourier transformed signals $X_1(f)$-$X_5(f)$ are the complex acoustic pressure signals with frequency. Modal decomposition, an advanced technique that uses an array of sensors to determine the specific modal amplitudes at the sensor array, can be used to determine the complex acoustic pressure of any cut-on acoustic mode in a duct. It is therefore proposed that one of the complex pressure signals $X_1(f)$-$X_5(f)$ can be replaced by the complex pressure signal of a specific mode travelling in a given direction in the test duct, $A^{\pm}_{m,n}$. For the two-source case, this technique could therefore be used to identify the contribution of both sources to the modal amplitudes at the sensor array used to decompose the modal content.

This technique makes use of the fact that assuming an incompressible and isentropic flow, stationary mean temperature and density and a constant axial mean flow profile, the Helmholtz equation (in cylindrical coordinates) can be expressed as the linear superposition of modal terms:

$$p(x,r,\varphi) = \sum_{m=-\infty}^{\infty}\sum_{n=0}^{\infty}(A^{+}_{m,n}e^{ik^{+}_{mn}x} + A^{-}_{m,n}e^{ik^{-}_{m,n}x})f_{m,n}(r)e^{im\varphi} \tag{8}$$

where $k^{-}_{m,n}$ and $k^{-}_{m,n}$ denote the axial wavenumbers, $A^{+}_{m,n}$ and $A^{-}_{m,n}$ denote the complex amplitudes for mode order (m,n), where m is the azimuthal mode order and n is the radial mode order. $f_{m,n}(r)$ is the modal shape factor for mode order (m,n), which is formulated by a combination of Bessel functions and is dependant on the cross-sectional geometry of the duct.

Bennett[11] advanced a modal decomposition technique based on Åbom's method,[12] whereby an array of microphones is mounted flush to the inner duct wall. The sensors in this array are equally spaced azimuthally and radially. The characteristics of this technique are:

1. incident and reflected modes can be identified;
2. a mean flow can be accommodated;
3. a frequency response function technique can be employed;
4. radial, as well as azimuthal, modes can be identified;
5. duct-wall flush-mounted microphones only are used for the decomposition;
6. the decomposition is performed for all frequencies not only at the BPF and harmonics;
7. data is acquired at all measurement locations simultaneously.

From the formulation of the acoustic pressure in a hard-walled duct given by Eq. 8, Bennett's modal decomposition technique is undertaken in two stages. In the first stage an azimuthal decomposition is carried out using microphones located circumferentially around the duct as follows:

$$p_{l,k} = \sum_{m=1-M}^{M-1} h_{m,k}e^{[jm\theta_l]} \quad \text{where} \quad \begin{array}{l} k = 0,1....2N-1 \\ l = 0,1,....2M-1 \\ \theta_l = \dfrac{2\pi l}{2M-1} \end{array} \tag{9}$$

This technique is repeated at different axial locations in order to decompose the pressure field into both the radial modal amplitudes and their incident and reflected components:

$$h_{mk} = \sum_{n=0}^{N-1}[A^{+}_{m,n}e^{-jk^{+}_{m,n}x} + A^{-}_{m,n}e^{+jk^{-}_{m,n}x}]f_{m,n}(r) \tag{10}$$

The first part of the technique requires 2 measurements per azimuthal wavelength ($\frac{2\pi}{m}$), analogous to the Nyquist sampling criterion. $2M_{max}+1$ sensors are therefore required to be located azimuthally, where

M_{max} is the maximum azimuthal mode to be decomposed. This places an upper frequency limit at which this technique can be applied for a given amount of acoustic sensors. Holste and Neise[13] make similar conclusions, and also state that aliasing is possible when not enough sensors are located per cut-on mode. A full expansion of this modal decomposition procedure can be found in chapter 7 of Bennett.[11]

With reference to Figure 1, the modal content of the noise radiated from sources S_1 and S_2 could be identified at sensor array A using the modal decomposition technique outlined above. The complex modal amplitudes for any mode order (m,n) which is cut-on in the frequency range of interest can then be found. The azimuthal index, m, of any mode to be decomposed must also be less than or equal to 2N-1, where N is the number of sensors per ring. These complex pressure sequences can be used to generate auto-spectra of each mode (m,n) by simply multiplying the complex amplitude of the mode by its complex conjugate. Similarly, cross-spectra can be formulated on a modal basis.

The complex acoustic pressure of each mode decomposed can be used as an output measurement, shown in place of Y_3 in Figure 7, in the five-microphone technique. Since the five-microphone technique uses the cross-spectra between five sensor measurements, the hypothesis is that one of these sensors can be replaced by the complex modal amplitude of a mode of interest. The time domain measurement signals y_1, y_2, y_4 and y_5 are transformed into the frequency domain, giving the complex pressure signals Y_1, Y_2, Y_4 and Y_5. The five-microphone technique could therefore be used to identify the contributions of sources S_1 and S_2 to the modal amplitudes at the location where the modes have been decomposed, using the auto and cross-spectra between these five complex pressure measurements as per equations 6 and 7. This technique could be used to identify how much acoustic energy each source contributes at a specific mode order over a frequency range of interest. This method could be applied in a real turboshaft engine to identify the contribution of noise sources inside the engine to the modal sound pressure levels at the engine exhaust, allowing a better understanding of the propagation of the sound from noise source to engine exhaust. This information can be used to optimise the design of acoustic liners to attenuate this sound field.

IV. Experimental Rig

The experimental set-up used to investigate the techniques outlined in section II and the CSA modal technique outlined in section III was designed as part of the TEENI (Turboshaft Engine Exhaust Noise Source Identification) project. The rig was built and tested at the Engine Acoustics branch of one of the consortium partners – DLR (German Aerospace Agency). The rig was designed to simulate the key acoustic elements of a turboshaft engine. The sources of noise in the rig are a single rotor-stator stage consisting of 24 rotor blades and 5 stator vanes and an array of sixteen loudspeakers which can be used to generate broadband, tonal or narrowband noise. The rotor speed can be set at 0, 1500 or 3000 rpm, and any number from one to sixteen loudspeakers can be switched on. The amplification factor of the loudspeakers can also be changed. A schematic of the rig design is shown in Figure 8. By varying these parameters, a wide variety of different test scenarios were investigated, allowing the classic techniques discussed in sections II and III to be tested for scenarios of noise source identification in turbomachinery.

Data was acquired at 256 independent ADC (analogue-to-digital) channels using in-house hardware and software at a sampling frequency of 16 kHz. G.R.A.S. Sound and Vibration condenser type 40BP microphones were used to acquire the acoustic pressures at the two arrays of receivers, one of which was located at the hub of the rig (hub-to-tip ratio, $\eta = 0.56$). Reference sensors were also located in the duct close to the loudspeakers and close to the rotor-stator stage. The two banks of 64 receivers can be used to modally decompose the pressure field at both axial locations.

To test the classic techniques outlined in section II, the sources of noise in the rig are the rotor rotating at 1500 rpm (giving a blade pass frequency of 605 Hz), and a single loudspeaker generating broadband noise. The rotor induces a mean flow in the positive x-direction of 9 m/s at the duct inlet at 1500 rpm. These noise source regions will be referred to as S_{rot} and $S_{LS,bbn}$ respectively. Each technique is used to attempt to identify the contribution of one or both of these sources to the sound pressure received at a sensor located in inlet array of sensors. Table 1 collates these tests points. In testing the classic techniques, test point 1 was the key test investigated. The aim of each of the techniques is to accurately identify the frequency content of one or both of these noise source regions to the noise received at a sensor from the inlet bank of sensors shown in (C) of Fig. 8. Test points 2 and 3 were used to provide benchmark spectra of each source's contribution to the noise at this inlet sensor, which could be used to assess the effectiveness of each technique. The results from this study are given in section V.

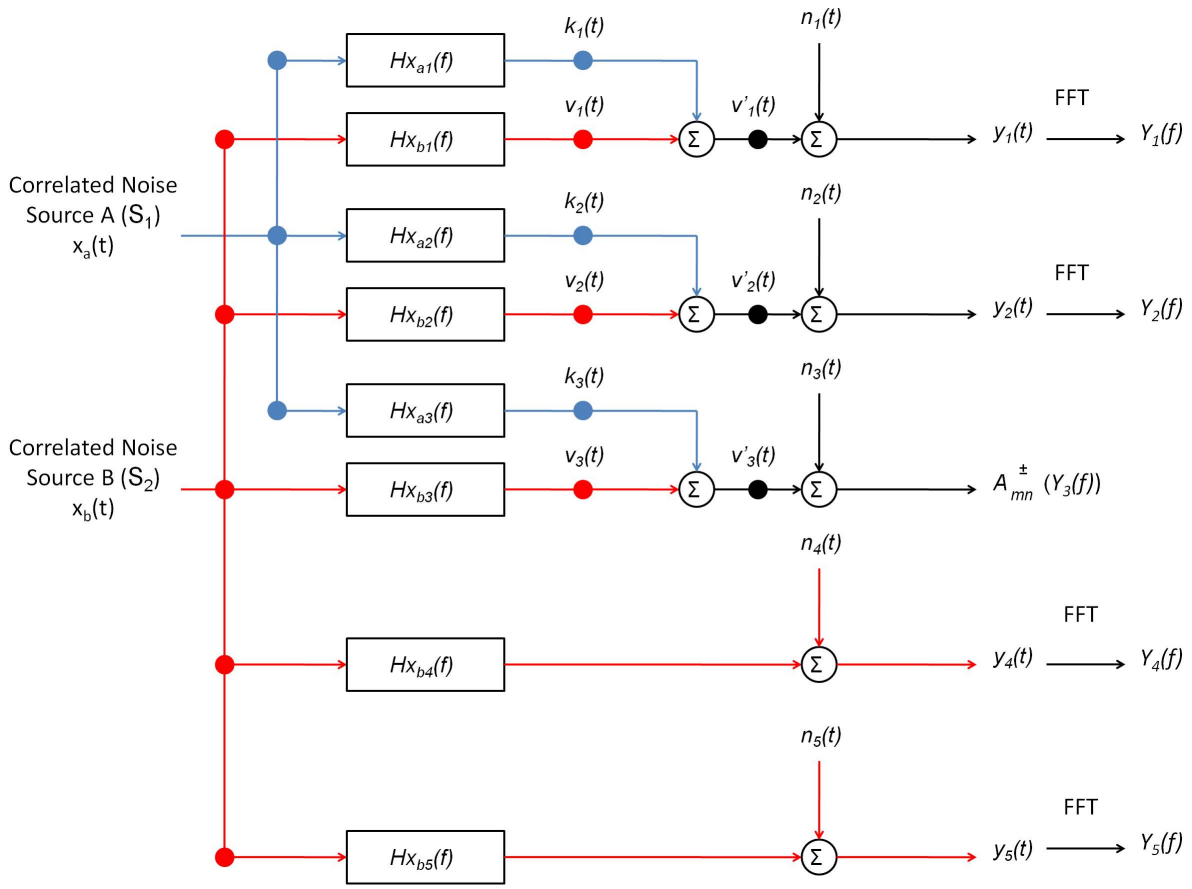

Figure 7: CSA modal five-microphone technique model for scenario shown in Fig. 1. Measurement $Y_3(f)$ has been replaced by $A^{\pm}_{mn}$, the complex modal amplitude of the (m,n) mode.

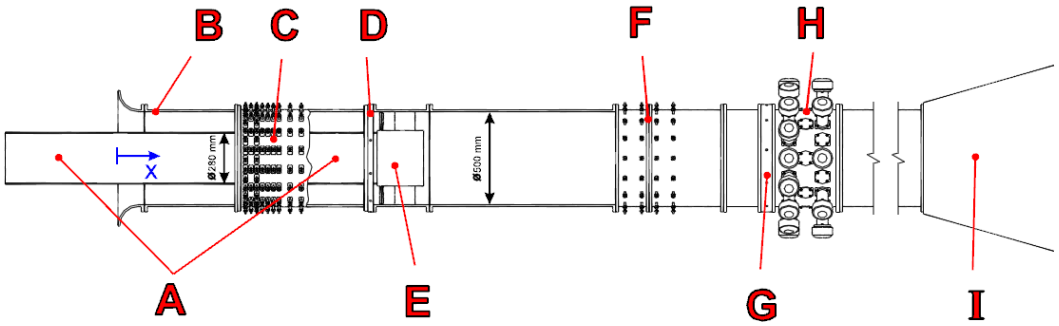

A: hub
B: inlet duct
C: inlet array
D: ring with reference sensors
E: rotor-stator stage
F: outlet array
G: ring with reference sensors
H: mode generator
I: anechoic termination

Figure 8: Schematic of DLR rig.

To test the new modal technique outlined in section III, a test point with two broadband noise source regions were investigated. The aim of the technique is to identify the contribution of the rotor and a single loudspeaker generating broadband noise to the modal content decomposed at the inlet bank of receivers shown in Fig. 8. The technique was tested to identify the contribution of two broadband noise sources (S_{rot} and $S_{LS,bbn}$) to the modal content at the duct inlet, using test point 1 shown in Table 1. The results of this investigation into broadband noise source identification using the newly developed CSA modal technique are shown in section VI.

Table 1: Test points investigated in order to test classic techniques and the novel modal based technique. There are two source regions which are adjusted between test points – an array of loudspeakers and a rotor-stator stage.

Test Point	Rotor-Stator Stage	Loudspeaker Array
1	Rotor rotating at 1500 rpm	Single loudspeaker generating broadband noise
2	–	Single loudspeaker generating broadband noise
3	Rotor rotating at 1500 rpm	–

V. Results from Classic Techniques

The following test results have demonstrated the relative effectiveness of each technique discussed in section II when applied to test scenarios investigated on the experimental rig described in section IV. With reference to Figure 8, the rotor is rotating at 1500 rpm. This noise source region will be referred to as S_{rot}. A single loudspeaker located at the mode generator generates broadband noise. This noise source will be referred to as $S_{LS,bbn}$. The key test point investigated has both sources S_{rot} and $S_{LS,bbn}$ present; test point 1 in Table 1. Two other test points; one with $S_{LS,bbn}$ only and the other with S_{rot} only, are used as benchmarks for the analysis of the efficacy of all noise source identification techniques tested. These are test points 2 and 3 as shown in Table 1.

The COP model shown in Figure 2 assumes no noise at the input, i.e. a pure source measurement. The input measurement, x, is taken from a sensor inside the loudspeaker cone. The output measurement, y, is taken from a sensor at the inlet bank of sensors. These sensor positions are shown in Figure 9. The v spectrum therefore shows the contribution of $S_{LS,bbn}$ to the noise at this inlet sensor. Since the source $S_{LS,bbn}$ is dominant inside the loudspeaker cone, the contribution of source S_{rot} at the inlet sensor is identified as extraneous noise. This result, shown in Figure 10, is compared with the auto-spectrum for the same inlet sensor when only $S_{LS,bbn}$ is present (test point 2 in Table 1). This spectrum can be used as a benchmark to examine the effectiveness of the COP result. The COP method is shown to be effective by the fact that these spectra match very well for all frequencies, demonstrating the usefulness of the technique when a pure source measurement is possible.

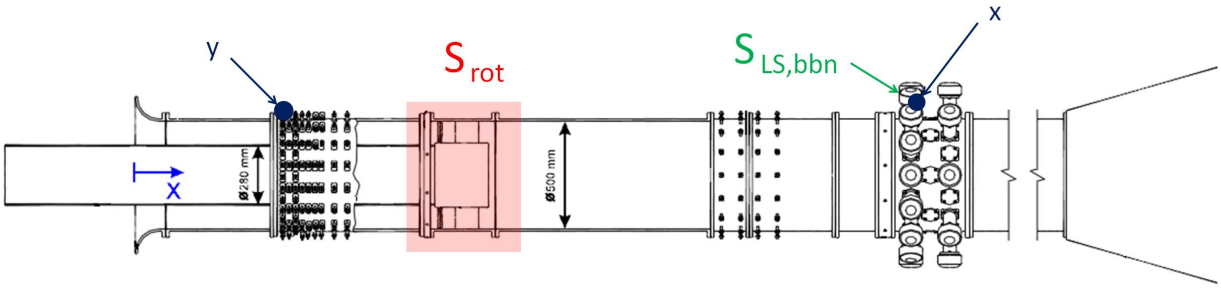

Figure 9: Locations of sensor measurements for identification of $S_{LS,bbn}$'s contribution to the noise measured at y, using the coherent output power technique.

In the results shown in Fig. 10, the coherent output power model was compared with the auto-spectrum at

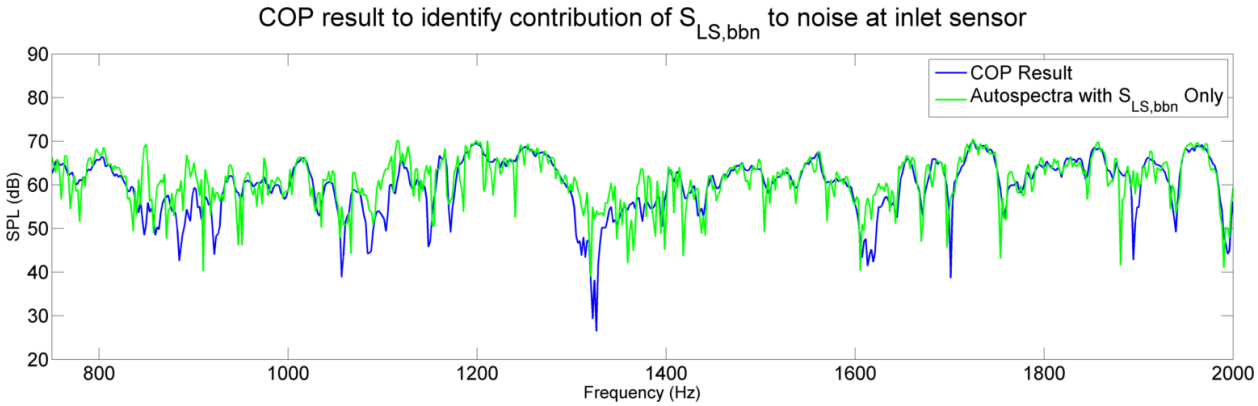

Figure 10: Coherent output power results for identification of contribution of $S_{LS,bbn}$ to the noise at an inlet sensor with both sources (S_{rot} and $S_{LS,bbn}$) on. The blue spectrum shows the coherent output result found using the measurement from a sensor in the loudspeaker cone as the source measurement, and the inlet sensor as the output measurement. The auto-spectrum at the same inlet sensor with $S_{LS,bbn}$ only is shown in the green spectrum for comparison.

the inlet sensor with $S_{LS,bbn}$ only present. This auto-spectrum was a convenient benchmark for evaluating the success of the COP technique. A similar benchmark was required to show the auto-spectrum at the same inlet sensor with S_{rot} only present – test scenario 3 in Table 1. However, due to the presence of flow noise induced in the test duct when S_{rot} is present, a raw auto-spectrum at the inlet sensor will contain the contribution of S_{rot} and any flow noise present. In order to give an accurate spectrum showing the contribution of S_{rot} only without flow noise contaminating the results, Chung's[2] signal enhancement method of flow-noise rejection was used to provide a suitable benchmark. The signal enhancement technique was applied using three sensors at the inlet bank with S_{rot} only, removing the uncorrelated flow noise and showing the contribution of S_{rot} to the inlet sensor of interest. Hence a flow-noise removed spectrum was found which could be used as a benchmark for comparison for any technique's results in measuring S_{rot}.

The coherent output power technique was used to attempt to identify the contribution of S_{rot} to the noise measured at the inlet sensor. The locations of the sensors used are shown in blue in Figure 11. The result of applying the COP technique in this test scenario is shown in Fig. 12. This COP result, shown in blue, matches the benchmark rotor-stator noise at the inlet sensor quite accurately (shown in green); however two main issues can be identified. The first is that the tonal peak at the first harmonic of the BPF at 1210 Hz has not been identified in the v spectrum. Secondly, the sound pressure level is overestimated by several dB at certain frequencies, such as in the range 1700 - 2000 Hz, which would contradict the expected result that the coherent output power would drop with the presence of uncorrelated noise at the input measurement.

The signal enhancement technique can be used when no pure measurement of the source of interest is available, provided any additional extraneous noise is uncorrelated between each sensor measurement. Due to the presence of flow noise at the sensor measurements, the signal enhancement technique may be considered more suitable than the coherent output power technique in this situation. The locations of the three sensors used are shown in Figure 11. The aim of this technique is to accurately identify the contribution of S_{rot} to the noise measured at y_1, which is the same sensor measurement as used as the y signal in the coherent output power technique. The result from application of the signal enhancement technique is shown in the red spectrum of Figure 12. A similar result is seen with the signal enhancement technique as with the coherent output power technique. The signal enhancement technique is expected to give a result uncontaminated by the uncorrelated flow noise. The SE spectrum however overestimates the flow noise-removed spectrum even more than the COP result. The first harmonic of the BPF tone at 1210 Hz however has been clearly identified in this case, which is a significant result.

As a consequence of the presence of a second correlated source, the coherent output power and signal enhancement techniques will not give an exact estimate of S_{rot} to the inlet sensor, but will give an estimate of a mixture of both sources S_{rot} and $S_{LS,bbn}$, despite the sensors used for measurements y_2 and y_3 being located close to the rotor. This means that the assumed COP model shown in Figure 3 will be inaccurate. Given the presence of a second correlated source, a more accurate COP model for this scenario is shown in

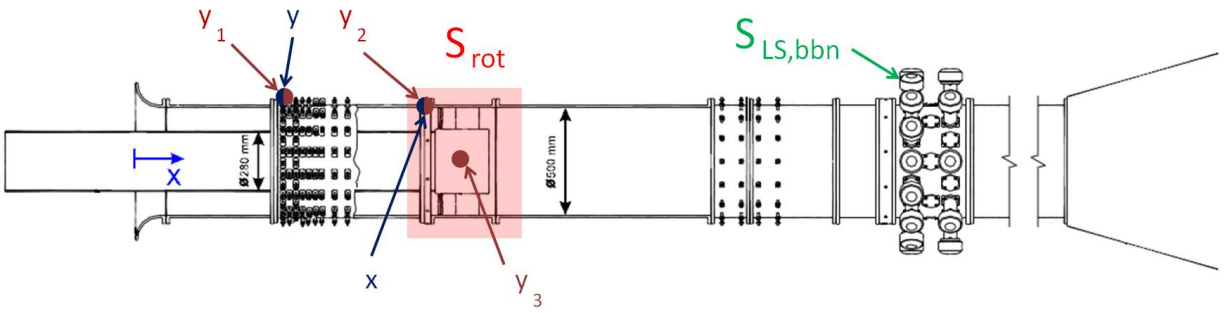

Figure 11: Locations of sensor measurements for identification of S_{rot}'s contribution to the noise measured at y. The sensors used for the coherent output power technique are shown in blue. The sensors used for the signal enhancement technique are shown in red. The aim of both techniques is to identify the contribution of S_{rot} to the noise measured by a sensor at the duct inlet – shown as sensor y for the COP technique and y_1 for the SE technique. This is the same inlet sensor in both cases.

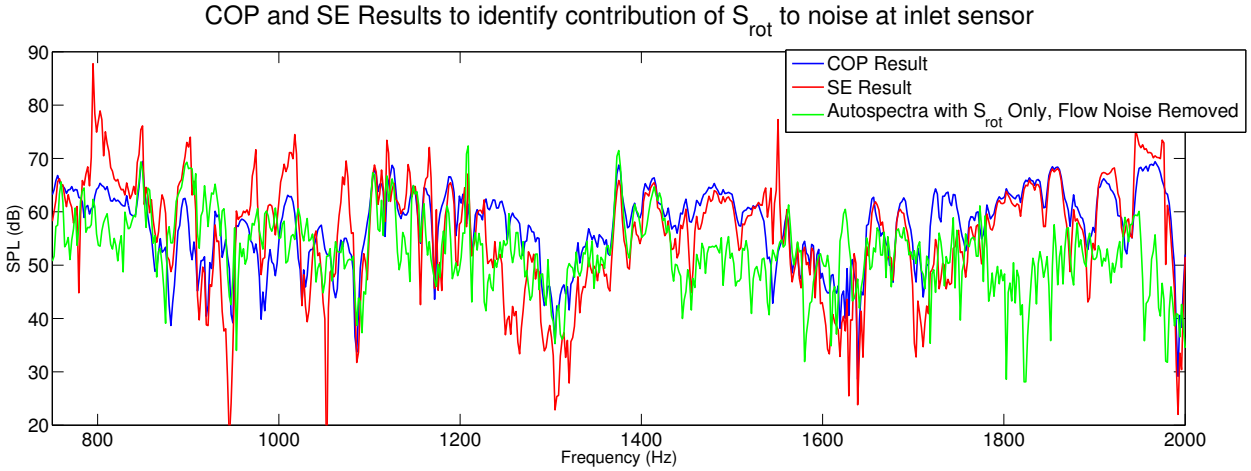

Figure 12: Coherent output power and signal enhancement results for identification of contribution of S_{rot} to the noise at inlet sensor with both sources on. Sensor positions are shown in Figure 11. The blue spectrum shows the coherent output result found using the measurement from a sensor near the rotor-stator as the source measurement, and the inlet sensor as the output measurement. The red spectrum shows the signal enhancement result using two sensors close to the rotor-stator and the same inlet sensor. The flow noise-removed spectrum at the same inlet sensor with S_{rot} only is shown by the green spectrum for comparison.

Figure 13. Figure 14 shows the auto-spectrum of measurement y_2 with S_{rot} only, $S_{LS,bbn}$ only and both S_{rot} and $S_{LS,bbn}$ to demonstrate the relative sound pressure levels of both sources. Since S_{rot} is the dominant source at the sensors close to the rotor-stator, the techniques still give a good measurement of the shape of the correct spectrum; however the presence of noise from $S_{LS,bbn}$ means the spectrum has a higher sound pressure level than expected. The COP and SE results from Fig. 12 are shown again in Fig. 15, but with the flow-noise removed spectrum at the inlet sensor with both sources present used as a benchmark for comparison to show how the techniques identify a mixture of both sources. Figs. 14 and 15 show that at frequencies where $S_{LS,bbn}$ has a sound pressure level near that of S_{rot} at the sensor (see Fig. 14), such as around 1500 Hz and 1800 Hz, both the COP and SE techniques spectra in Fig. 15 have sound pressure levels which match the levels of the $S_{LS,bbn}$ only auto-spectrum in Fig. 14.

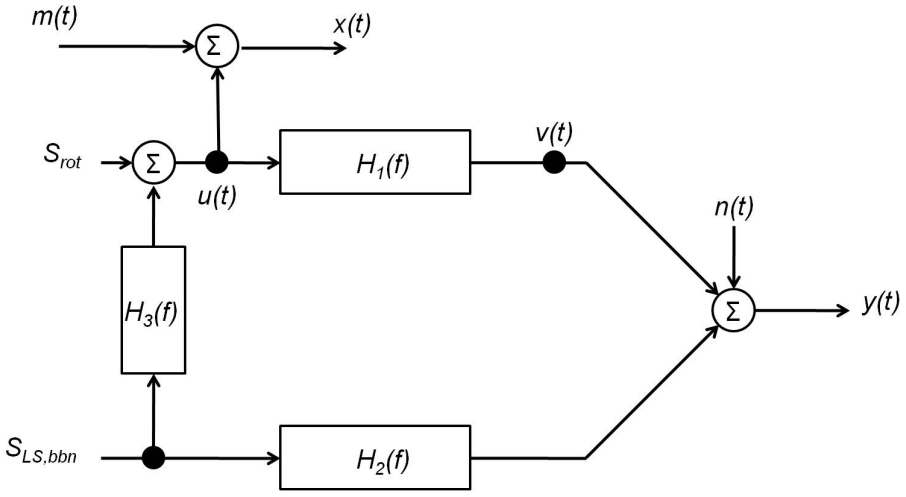

Figure 13: Model for COP technique when used to attempt to identify the contribution of S_{rot} to the noise at sensor y as shown in Fig. 11. The source measurement, $x(t)$, located near the rotor-stator stage, S_{rot}, also measures a contribution from $S_{LS,bbn}$.

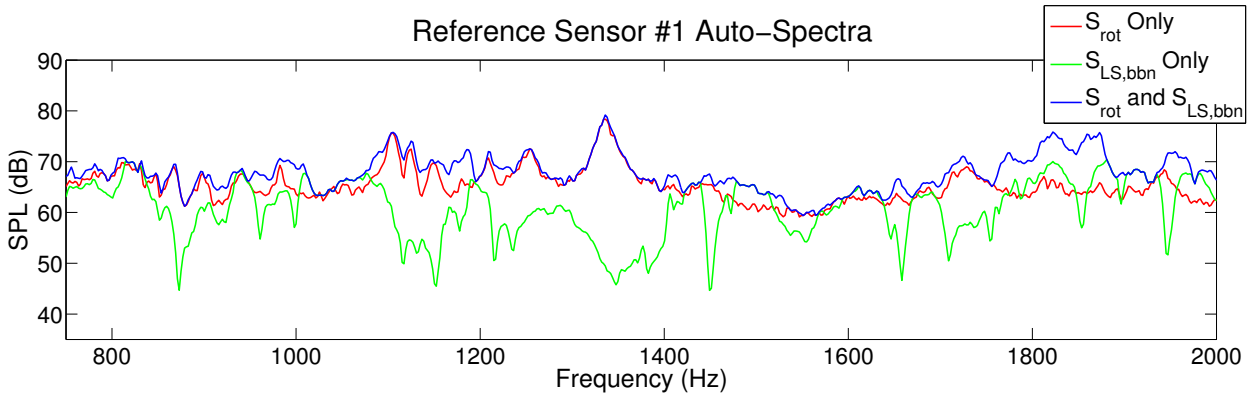

Figure 14: Auto-spectra of acoustic sensor measurement used as y_2 in the signal enhancement technique and x in the coherent output power technique. This figure shows the relative sound pressure levels of S_{rot} and $S_{LS,bbn}$.

In order to decouple both sources, a partial coherence formulation is required. This partial coherence formulation is discussed in section II. The five-microphone conditional spectral analysis technique developed by Hsu and Ahuja[4] discussed in section II is a technique which applies the partial coherence formulation given by Bendat and Piersol[14] to separate out the contributions of two sources. Two source measurements of one source are required; the source measurements in this case must read one source only and can accommodate extraneous noise, provided this extraneous noise is uncorrelated with the noise at any other sensor. These source measurements are taken from sensors inside the loudspeaker cone, giving two source measurements

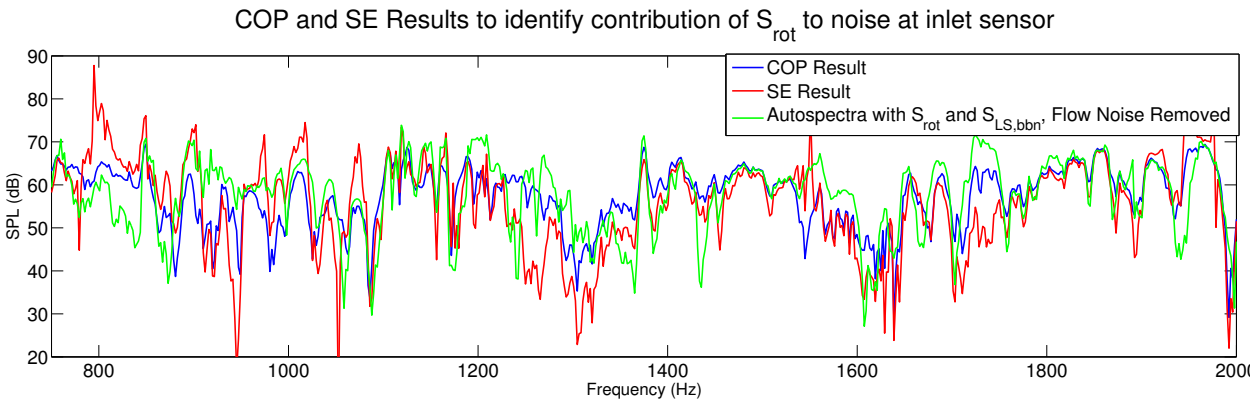

Figure 15: Results for identification of S_{rot}'s contribution to the noise at the inlet sensor using COP and SE techniques, showing how both techniques fail as they measure a combination of both sources.

of $S_{LS,bbn}$ (y_4 and y_5). The locations of these measurement signals are shown in Figure 16. The other three sensors are located close to the rotor-stator (y_1 and y_2) and located at the inlet duct (y_3). This technique gives three spectra of interest: the v spectrum showing the contribution of $S_{LS,bbn}$ to the noise at the inlet sensor, the k spectrum showing the contribution of S_{rot} to the noise at the inlet sensor, and the n spectrum which gives the remaining contribution to the acoustic pressure. The k and v spectra results are shown in Figs. 17 and 18 respectively. Deductive thinking would suggest that the noise spectra, which contains any noise present in the raw y spectra not accounted for by the v and k spectra, will contain the contribution of flow noise to the inlet sensor measurement. This noise spectrum is therefore compared to the spectrum of the flow noise, which was found by subtracting the PSD of the flow-noise removed spectrum of the inlet sensor from the raw PSD of the inlet sensor. This result is shown in Fig. 19.

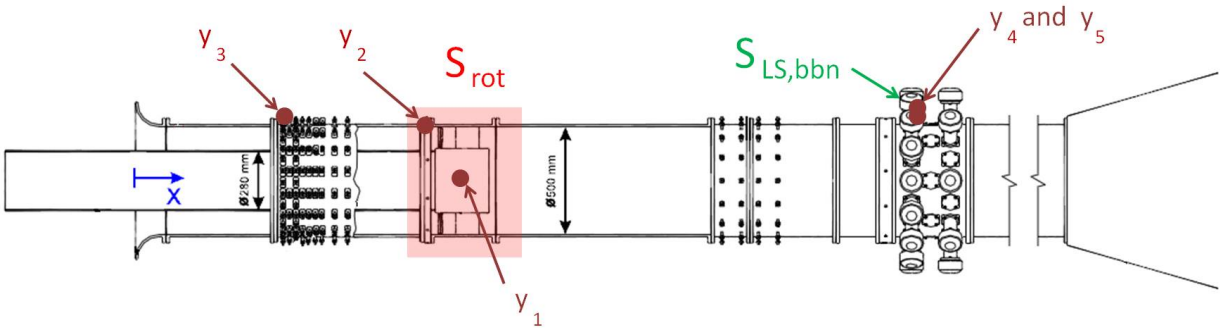

Figure 16: Locations of sensor measurements for identification of $S_{LS,bbn}$ and S_{rot}'s contribution to the noise measured at y_3, using the five-microphone conditional spectral analysis technique.

The partial coherence formulation underpinning this technique has successfully decoupled both sources, and accurate spectra have been obtained showing the contributions of both sources to the noise at a sensor of interest. Furthermore, given that only two sources are present, the contribution of an additional uncorrelated noise can be found. Such uncorrelated noise in a real turboshaft engine could be flow noise. In the case of Fig. 18, the result closely matches the COP result in Fig. 10. This is due to the fact that the five-microphone CSA technique utilises the COP technique in its first stage, as discussed in section II. It is therefore crucial that the microphones used as measurements y_4 and y_5 are located such that they measure one source and uncorrelated noise only. If this requirement is not met, the technique will fail. The impact of a less precise source measurement by y_4 and y_5, as well as the impact of additional noise sources, will be quantified in future work.

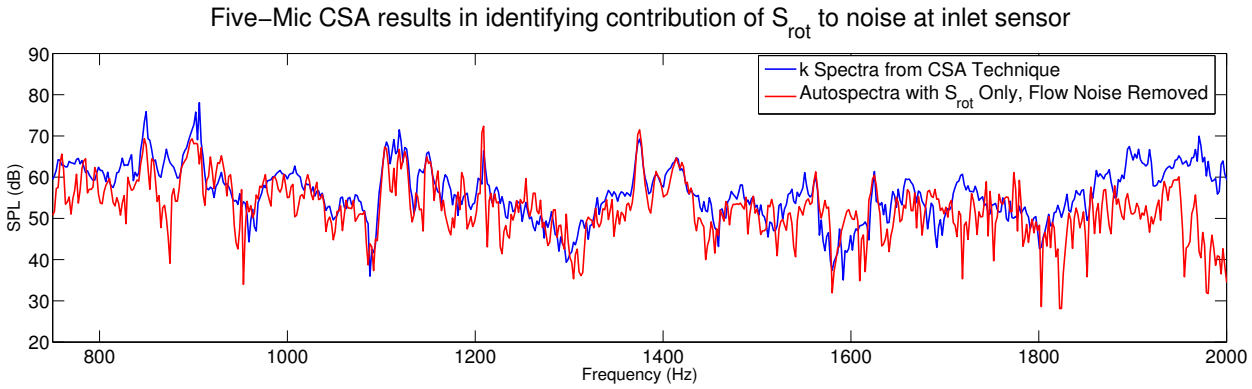

Figure 17: Results for identification of S_{rot}'s contribution to the noise at the inlet sensor using the five-mic CSA technique.

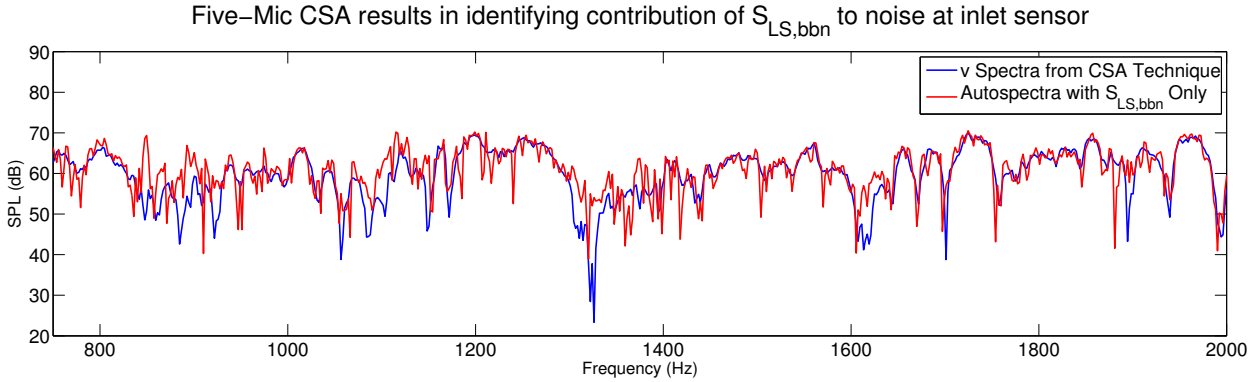

Figure 18: Results for identification of $S_{LS,bbn}$'s contribution to the noise at the inlet sensor using the five-mic CSA technique.

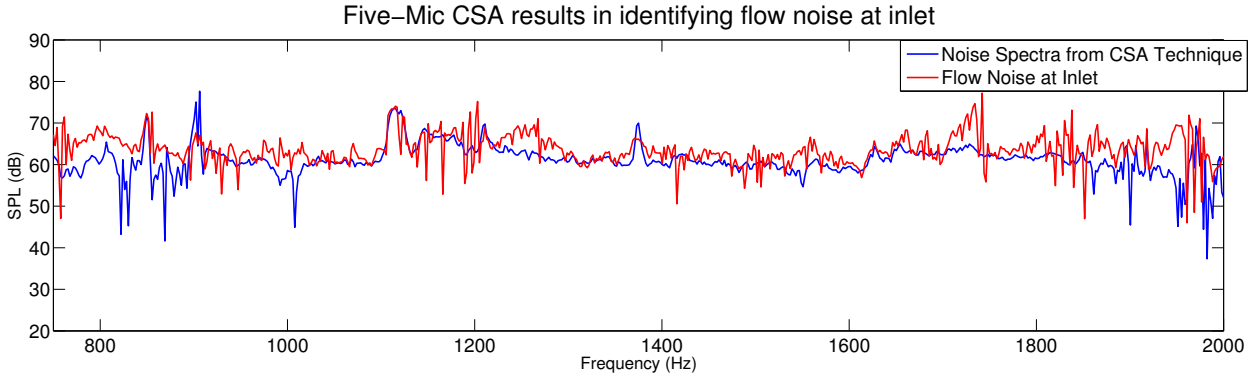

Figure 19: Results for identification of the hydrodynamic flow noise induced by the inlet sensor using the five-mic CSA technique.

VI. Results from Modal CSA Technique

The new modal CSA technique outlined in section III was tested for the cases of identification of tonal or broadband noise from two noise sources. The aim of this technique is to identify the contribution of one or more sources to the modal content received at the inlet of the test duct, which is analogous to the duct exhaust of a real turboshaft engine. In order to test this new technique, the modal content was first decomposed at the inlet with both sources in isolation. This gives the specific contribution of each source to the amplitudes of any cut-on modes. These amplitudes were used as the benchmark to test the technique's performance.

As with the classic five-microphone CSA technique results given in section V, five outputs are required for the modal CSA technique. Two of these outputs must measure one of the sources without measuring the other source of interest. Any additional extraneous noise measured by these sensors must not be correlated with any other sensors. The same sensor measurements y_1, y_2, y_4 and y_5 are used as in the classic CSA technique for testing the novel technique enhanced with modes. The sensor measurement y_3 was replaced with a complex modal amplitude decomposed at the inlet sensor bank. These sensor positions are shown in Figure 20. The approach used in this technique is described in section III. The Fourier transform is taken of the time-domain measurements y_1, y_2, y_4 and y_5, giving the frequency domain signals Y_1, Y_2, Y_4 and Y_5. The complex signal $A^{\pm}_{mn}$, which is the complex modal amplitude of the (m,n) mode travelling in the positive or negative x-direction, is used as measurement Y_3. This modal amplitude is found using the technique of modal decomposition at the inlet bank of receivers. All five outputs Y_1-Y_5 are complex frequency-domain measurements of the acoustic pressure. By calculating the auto and cross-spectra of these signals and applying equations 6 and 7, a total of nine spectra can be determined. These spectra are v_{1-3}, k_{1-3} and n_{1-3}. By examining the v_3, k_3 and n_3 spectra, the technique can be used to identify the contribution of two sources to the modal amplitude $A^{\pm}_{m,n}$.

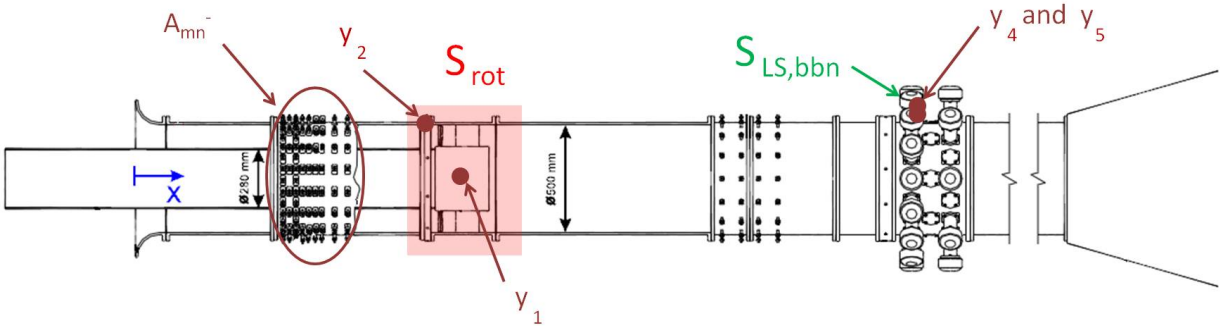

Figure 20: Locations of output measurements used in the modal CSA technique. The aim of this technique is to identify the contribution of S_{rot} and $S_{LS,bbn}$ to the amplitudes of the modes travelling in the negative x-direction, as measured by a bank of sensors at the duct inlet – shown as $A^{-}_{m,n}$.

Figure 21 a) shows the decomposed radial modal amplitudes with a single loudspeaker generating broadband noise ($S_{LS,bbn}$) in isolation (i.e. no other sources are present). Figure 21 b) shows the decomposed modal amplitudes with the rotor rotating at 1500 rpm (S_{rot}) in isolation. At any given frequency, the highest order cut-on modes dominate slightly. For the case of the rotor noise shown in Figure 21 b), the tonal peak at 605 Hz corresponds to the blade pass frequency of the rotor. These modal amplitudes are measured for modes travelling in the negative x-direction, i.e. travelling away from both sources and towards the entrance plane of the duct.

In order to test the modal CSA technique for the case of broadband noise sources, the same test point as used in section V was examined. This is shown as test point 1 as shown in Table 1. The results presented herein are taken at a specific mode order: the (2,0) mode. Any cut-on mode in the frequency range tested (200-2100 Hz) could have been selected. 2100 Hz represents the upper frequency limit of modal decomposition at the inlet of the test duct, given that there are 16 sensors per ring in the sensor array. The modal decomposition technique also allows the modal content of the pressure field to be decomposed with directionality (see section III), so $A^{+}_{2,0}$ or $A^{-}_{2,0}$ could be chosen as the mode of interest. $A^{-}_{2,0}$ was chosen as this represents the acoustic mode travelling away from the noise sources towards the inlet plane of the test

duct.

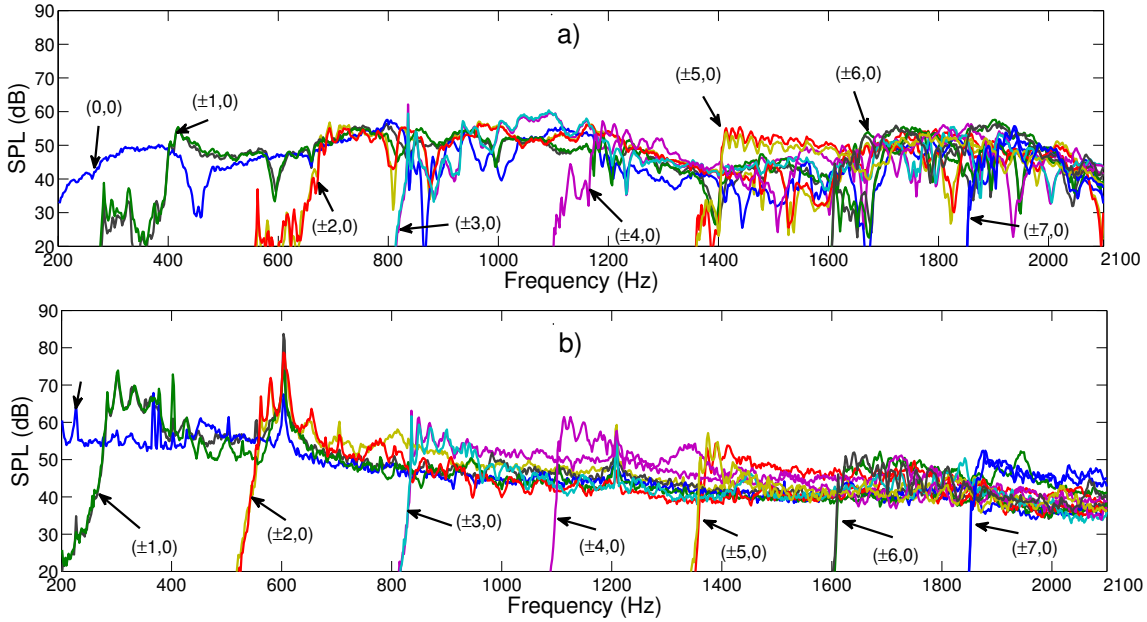

Figure 21: Spectra of modal amplitudes decomposed at the inlet sensor bank for all modes cut-on in the frequency range of interest when each source is present in isolation. The modes are travelling in the negative x-direction i.e. away from both sources and towards the inlet plane of the test duct (see Fig. 8). Figure a) shows the modal amplitudes when $S_{LS,bbn}$ is present in isolation. Figure b) shows the modal amplitudes when S_{rot} is present in isolation.

The complex modal amplitude of the $A^{-}_{2,0}$ mode decomposed at the inlet sensor bank was used as measurement Y_3 in the modal CSA technique. With reference to Figure 7, the k_3, v_3 and n_3 spectra identified using the technique are compared with the modal amplitudes decomposed when each source is present in isolation (see Figure 21). As discussed in section II, the five-microphone CSA technique is formulated in two stages. The first stage uses the coherent output technique. Figures 5 and 7 demonstrate how the v_3 spectrum, which identifies the contribution of $S_{LS,bbn}$ to the $A^{-}_{2,0}$ modal amplitude, is found using this coherent output power formulation. The second stage of the five-microphone CSA technique uses a partial coherence formulation of the signal enhancement technique, which is applied to the residual from the first stage. The k_3 and n_3 spectra found in this stage of the technique identify the contribution of the second correlated noise source (S_{rot}) to $A^{-}_{2,0}$, and any uncorrelated extraneous noise, respectively.

The v_3 spectrum is compared to the modal amplitude measured when only $S_{LS,bbn}$ is present in Figure 22. The blue spectrum shows the modal amplitude decomposed when both noise sources are present – Y_3 in Figure 7. The green spectrum shows the modal amplitude decomposed when only the loudspeaker is present ($S_{LS,bbn}$). The red spectrum shows the contribution of $S_{LS,bbn}$ to the modal content decomposed at the inlet, as identified using the CSA technique. This result can be compared to the green spectrum to verify the efficacy of the technique. The results are very positive, with both spectra matching well for all frequencies above modal cut-on. The technique overestimates the modal amplitude around the blade-pass frequency of 605 Hz, most likely caused by y_4 and y_5 measuring some of the blade-pass frequency acoustic energy generated by the rotor which propagates in the duct. However, it should be noted that although some of this BPF energy is being measured incorrectly in this result, the measured BPF tone is 20 dB below the actual BPF, which is a factor of 10. The overall result is therefore still very positive.

In section V, the noise spectrum of the classic five-microphone CSA technique (without modes) was compared to the spectrum of flow noise, see Fig. 19. This flow noise spectrum was found by first finding the flow-noise removed PSD of the inlet sensor. This PSD was found by applying the signal enhancement technique using the inlet sensor of interest and two adjacent sensors. By subtracting the flow-noise removed PSD of the inlet sensor from the raw PSD at the inlet sensor, the contribution of flow noise to the inlet sensor was found. In the modal decomposition technique, 64 sensors are used, however there are an additional 16 sensors in the inlet sensor bank that are not used to decompose the modal amplitudes. It was thought that

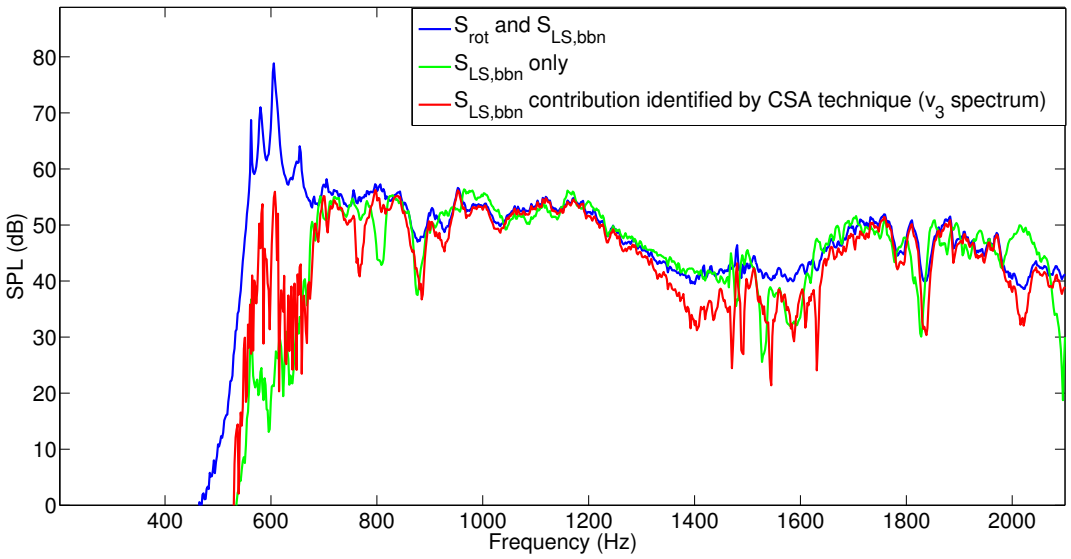

Figure 22: Spectra of the $A^{-}_{2,0}$ mode when both S_{rot} and $S_{LS,bbn}$ are present, shown in the blue spectrum (Y_3), and the spectra of the same mode order when $S_{LS,bbn}$ is present in isolation, shown in the green spectrum. The red spectrum shows the contribution of $S_{LS,bbn}$ to the amplitude of this mode order identified when both sources are present (v_3).

two of these unused sensors could be used to remove the flow noise from the decomposed modal content at the inlet sensor bank to find the flow-noise removed modal amplitudes. This would remove any noise uncorrelated between the modes and these sensor measurements. The contribution of extraneous flow-noise to these modal amplitudes could then be found and compared to the noise spectrum identified by the new modal CSA technique; the n_3 spectrum. Furthermore, the flow-noise removed modal spectra could be compared to the k_3 spectrum – the identified contribution of S_{rot} to the decomposed modal content.

The k_3 spectrum is compared to the $A^{-}_{2,0}$ modal amplitude measured when only S_{rot} is present (with flow noise removed) in Figure 23. The blue spectrum again shows the Y_3 spectrum. The green spectrum shows the modal amplitude decomposed when only rotor noise is present (S_{rot}), with uncorrelated flow noise removed using the signal enhancement technique. The red spectrum shows the contribution of S_{rot} to the modal content decomposed at the inlet, as identified using the CSA technique, when both $S_{LS,bbn}$ and S_{rot} are present. The technique again works well in this case. The accurate identification of the tonal peak at the rotor BPF at 605 Hz is a particularly good result. This is to be expected as the tonal energy at the blade-pass harmonics will propagate with high coherence in the test duct, hence the accurate result at these frequencies. At frequencies other than the BPF the shape of the identified rotor noise spectrum matches the shape of the rotor broadband noise quite well, with a discrepancy from the actual rotor broadband noise of around 3 dB at frequencies where the rotor broadband noise is significant. When the rotor broadband noise drops below around 30 dB, the identified contribution of the rotor is less accurate due to the poor signal-to-noise ratio as the loudspeaker ($S_{LS,bbn}$) dominates at these frequencies.

Figure 24 shows the n_3 spectrum in red, which is the contribution of extraneous noise to the amplitude of the $A^{-}_{2,0}$ mode decomposed at the duct inlet. This spectrum will contain any extraneous noise such as any flow noise present in the measurements. As explained above, the contribution of extraneous flow-noise to these modal amplitudes can be compared to the identified noise spectrum found by subtracting the PSD of a flow-noise removed modal spectrum from the raw modal spectrum PSD. This noise spectrum will identify the contribution of extraneous noise, such as flow noise and any ambient noise present in the tests. This spectrum is shown in green. As in the classic CSA technique, the extraneous flow noise identified by both the modal CSA technique when both sources are present and the signal enhancement technique when S_{rot} is present in isolation match well for all frequencies.

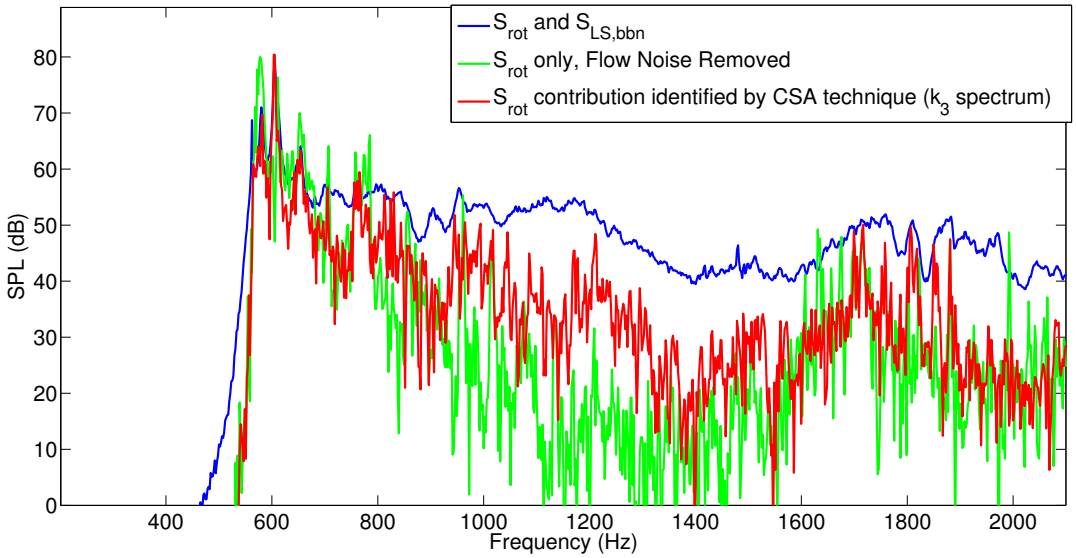

Figure 23: Spectra of the $A^{-}_{2,0}$ mode when both S_{rot} and $S_{LS,bbn}$ are present, shown in the blue spectrum (Y_3). The spectrum of the same mode order when S_{rot} is present in isolation, with flow noise removed using the signal enhancement technique, is shown in the green spectrum. The red spectrum shows the contribution of S_{rot} to the amplitude of this mode order identified when both sources are present (k_3).

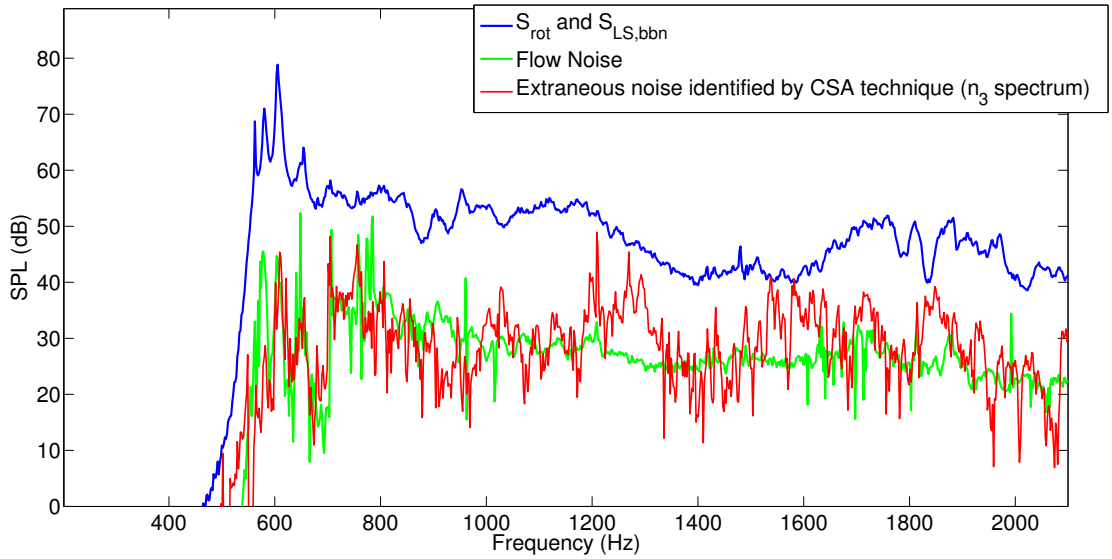

Figure 24: Spectra of the $A^{-}_{2,0}$ mode when both S_{rot} and $S_{LS,bbn}$ are present, shown in the blue spectrum (Y_3). The green spectrum shows the noise spectrum found by subtracting the flow-noise removed PSD from the raw PSD when S_{rot} is present in isolation. The red spectrum shows the extraneous noise contribution to the amplitude of this mode order identified when both sources are present (n_3).

VII. Conclusions

Classic techniques of noise source identification, which apply the coherence function between a number of sensor measurements, have been investigated for their applicability to turbomachinery noise source identification using experimental data. These techniques are pre-existing in the literature; however they had not been applied to the two noise region source scenario investigated in this paper. It was demonstrated that the five-microphone CSA technique was best suited to this scenario, as it is required to decouple both noise sources using a partial coherence formulation. This technique is applied in two stages; the first stage is performed by applying the coherent output technique, the second stage applies a partial coherence formulation of the signal enhancement technique on the residual. A novel modal CSA technique was also developed and tested using experimental data, which enhances the original five-microphone CSA technique by allowing the specific contribution of both noise sources to the modal content decomposed at the duct inlet to be identified.

Acknowledgements

This work was supported by the Seventh Framework Programme TEENI project which is funded under EU commission grant agreement 212367. The contribution of Mr Ulf Tapken, Mr Benjamin Pardowitz and Mr Philip Kausche to the experimental testing is gratefully acknowledged.

References

[1]W.G. Halvorsen and J.S. Bendat. Noise source identification using coherent output power spectra. *Journal of Sound and Vibration*, 9(8):15–24, 1975.

[2]J.Y. Chung. Rejection of flow noise using a coherence function method. *The Journal of the Acoustical Society of America*, 62:388, 1977.

[3]B.N. Shivashankara. High bypass ratio engine noise component separation by coherence technique. *Journal of Aircraft*, 20(3):236–242, 1983.

[4]J.S. Hsu and K.K. Ahuja. A coherence-based technique to separate ejector internal mixing noise from farfield measurements. In *4th AIAA/CEAS Aeroacoustics Conference, Toulouse, 2-4 June*, 1998.

[5]T. Minami and K.K. Ahuja. Five-Microphone Method for Separating Two Different Correlated Noise Sources from Farfield Measurements Contaminated by Extraneous Noise. In *9th AIAA/CEAS Aeroacoustics Conference, Hilton Head, South Carolina, May 1214*, pages 12–13, 2003.

[6]D.K. Nance. *Separating contributions of small-scale turbulence, large-scale turbulence, and core noise from far-field exhaust noise measurements*. PhD thesis, Georgia Institute of Technology, 2007.

[7]G. Bennett and J.A. Fitzpatrick. A comparison of coherence based acoustic source identification techniques. In *12th International Congress on Sound and Vibration, Lisbon, Portugal*, volume 11, page 14, 2005.

[8]G. Bennett and J.A. Fitzpatrick. Noise source identification for ducted fan systems. *American Institute of Aeronautics and Astronautics*, 46:1663–1674, 2008.

[9]G. Bennett, J. Mahon, and J.A. Fitzpatrick. Non-linear identification applied to broadband turbomachinery noise. In *12th CEAS-ASC Workshop on Turbomachinery Broadband Noise, Bilbao, Spain, 23-24 October*, 2008.

[10]G. Bennett, I. Davis, U. Tapken, and J. Mahon. Non-linear frequency scattering of broadband noise in turbomachinery. In *16th AIAA/CEAS Aeroacoustics Conference, Stockholm, 7-9 June*, 2010.

[11]G. Bennett. *Noise Source Identification For Ducted Fans*. PhD thesis, Trinity College Dublin, 2006.

[12]M. Åbom. Modal decomposition in ducts based on transfer function measurements between microphone pairs. *Journal of Sound Vibration*, 135:95–114, 1989.

[13]F. Holste and W. Neise. Noise source identification in a propfan model by means of acoustical near field measurements. *Journal of Sound and Vibration*, 203(4):641–665, 1997.

[14]J.S. Bendat and A.G. Piersol. Random data analysis and measurement procedures. *Measurement Science and Technology*, 11:1825–1826, 2000.

[15]J.M. Tyler and T.G. Sofrin. Axial compressor noise studies. *SAE Transactions*, 70:309–332, 1962.